J. Fluid Mech. (1999), *vol.* 393, *pp.* 241–256. Printed in the United Kingdom

Resonant acoustic frequencies of a tandem cascade. Part 2. Rotating blade rows

By B. M. WOODLEY AND N. PEAKE

Department of Applied Mathematics and Theoretical Physics, University of Cambridge, Silver Street, Cambridge CB3 9EW, UK

(Received 12 November 1998 and in revised form 15 March 1999)

In Part 1 (Woodley & Peake 1999) we described a method for predicting the occurrence of resonant states in a system comprising twin cascades in zero relative motion. We now demonstrate how that work can be extended to account for the case of more practical interest, in which the upstream cascade (rotor) is rotating in the transverse direction relative to the downstream cascade (stator). Time periodicity now forces the temporal frequency of any disturbance to be an integer multiple of the rotor passing frequency in the stator frame, and vice versa, and this leads to the requirement to sum over a discrete set of temporal modes, as well as over the spatial modes already described in Part 1. The mechanisms by which temporal and spatial modes are scattered by the blade rows is made clear by the analytical approach adopted here; the scattering of the incident pressure (and, for the stator, vorticity) fields by each row in its own frame is completed using results similar to those presented in Part 1, and the fields in the two frames then matched across the inter-row gap to provide a single matrix equation. Specimen results for the conditioning of this equation are given, and although it seems more difficult to obtain very strong excitation than it was for zero rotation, the significance of Parker resonance of the stator is again apparent.

1. Introduction

In Part 1 (Woodley & Peake 1999) the natural resonant frequencies of a tandem cascade were determined when there is zero relative rotation. Here we show how to extend that analysis to the practical case in which the rotor rotates relative to the stator, and it turns out that the scattering theory developed in (1) can again be applied, once the transformation of the unsteady field between the rotating and non-rotating frames has been completed.

In § 2 we present the problem formulation, and in particular describe the Tyler–Sofrin (1962) condition on the unsteady field, which arises as a consequence of the temporal and spatial periodicity forced on the system by the relative rotation. The field in the gap between the blade rows comprises vortical and pressure waves, and the way in which these modes transform between the two frames is described in § 3. In § 4 the application of the analysis from (1) to the scattering by the rotor and stator is described, and in § 5 sample results are presented. It will be seen that it is more difficult to excite the rotating system than was found for zero relative motion in (1), but the significance of Parker resonances of the stator will again be apparent. The analysis described here has much in common with work by Hanson (1992, 1993, 1994), who considered the inhomogeneous problem of forced motion in a rotor–stator system. Part of that study described the possible trapping of acoustic modes

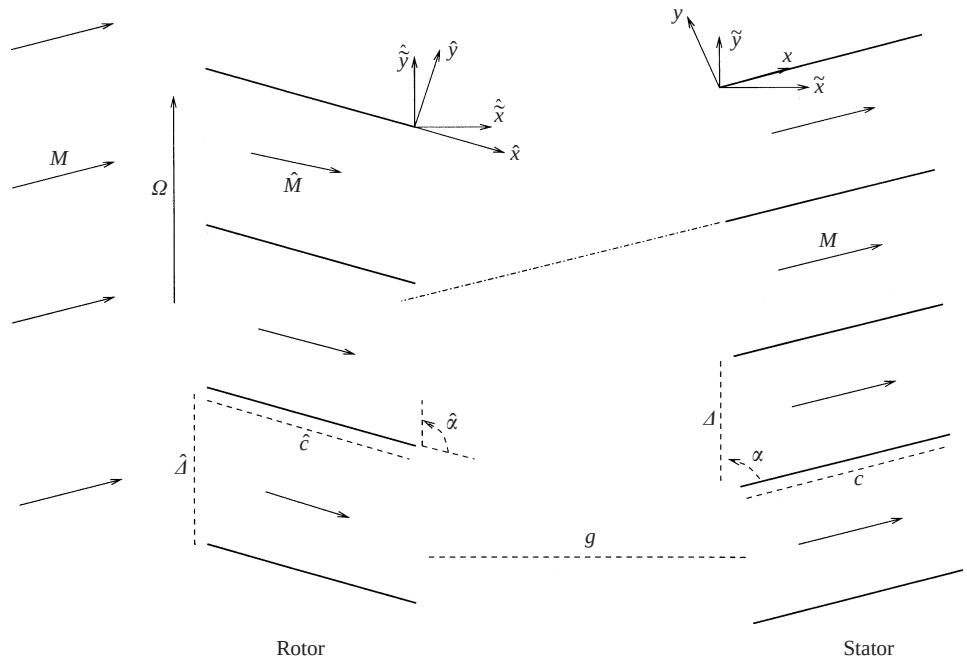

FIGURE 1. Rotating twin cascade system. $\hat{M}$ is the Mach number in the rotor frame. The dash-dot line represents the passage of vortical gusts from the rotor to a given stator leading edge.

by the rotor swirl, but this point will not be discussed further here, since it has not proved possible to account for the corresponding turning of the steady flow within our analytical scheme. We also note that recent, related work has been completed by Linton & McIver (1998), who determine resonant modes for static, radial fins spanning a circular cylindrical duct, with zero flow.

2. Problem formulation

2.1. *Geometry*

We consider a rotating blade row (rotor) containing B blades, located upstream of a stationary blade row (stator) containing V blades (conventionally termed vanes), and analyse the linear twin cascade formed by unwrapping the blade row at radius r^* (superfix * denoting dimensional variables), so that the radial direction is transformed into the spanwise direction – see figure 1. This is a standard approximation in turbomachinery theory, and relies on the fact that in typical situations the curvature of the duct passage containing the blades is small; specifically, if the blade tip radius is r_2^* and the hub radius is r_1^* we require $(r_2^* - r_1^*)/r_1^* \ll 1$. The leading-edge spacings in the rotor and stator are denoted as $\hat{\Delta} r^*$ and Δr^* respectively (the superfix $\hat{}$ will be used to denote rotor variables), and by considering the number of blades which must fit into each row we see that $\Delta = 2\pi/V$ and $\hat{\Delta} = 2\pi/B$. There is a steady axial flow through the cascade of speed Mc_∞^*, with c_∞^* the uniform-flow sound speed, and the rotor rotates with shaft rotation speed Ω_s^* relative to the stator. We assume that both the rotor and the stator blades are aligned exactly parallel to their respective local steady flow directions (so in particular the stator blades are aligned with the axial flow), and since we also assume that all blades have zero thickness and camber,

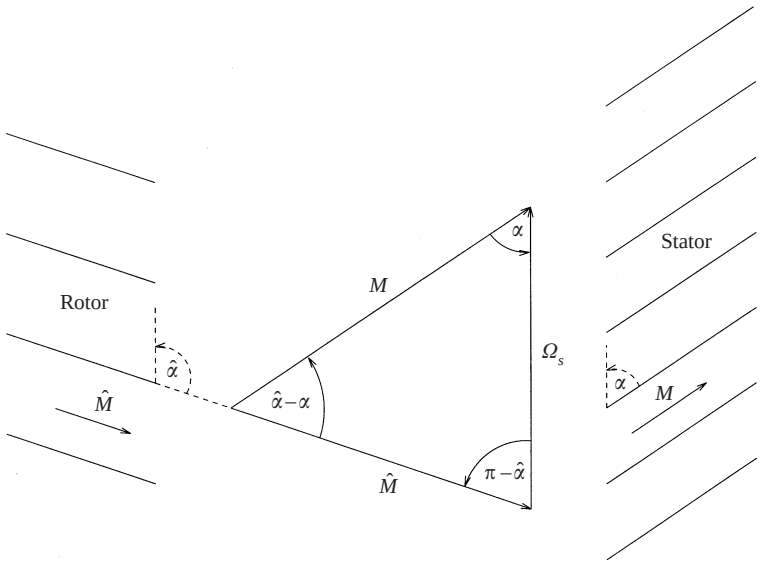

FIGURE 2. Mean flow velocity triangle.

it follows that the steady flow throughout the system is uniform. This requirement forces the stagger angles of the rows and the flow speeds through the rows to obey the velocity triangle shown in figure 2, from which it is clear that $\hat{M}$, the Mach number of the steady flow in the frame moving with the rotor, is given by

$$\hat{M}^2 = M^2 + \Omega_s^2 - 2M\Omega_s \cos\alpha. \tag{2.1}$$

Here $\Omega_s \equiv \Omega_s^* r^*/c_\infty^*$, and α is the stator stagger angle. A similar expression involving the rotor blade stagger angle, $\hat{\alpha}$, can also be determined.

In what follows we will need to non-dimensionalize the various flow quantities, and we choose to non-dimensionalize lengths by the annular radius of the cascade r^*. In (1) velocities were non-dimensionalized using the steady flow speed relative to the blade rows, which in that zero-rotation case is of course the same for each blade row. In order to use results from (1) in this paper we must continue to non-dimensionalize velocities using the steady flow speed relative to the particular blade row under consideration, i.e. $c_\infty^*\hat{M}$ for the rotor and $c_\infty^* M$ for the stator. It therefore follows that the rotor and stator flows will require different velocity scales, and this will necessitate some care when the separate rotor and stator scattering problems are matched together. As well as the velocity scales being different, it follows that the time scales in the rotor and stator frames, $r^*/c_\infty^*\hat{M}$ and $r^*/c_\infty^* M$ respectively, are also different, and we denote non-dimensional time in each frame by $\hat{t}$ and t respectively. In addition to non-dimensionalizing the shaft rotation rate using the sound speed, as in (2.1), it will also prove convenient to non-dimensionalize it with respect to the flow velocity scale in each frame separately, leading to $\Omega_s^s \equiv \Omega_s/M$ in the stator frame and $\Omega_s^r \equiv \Omega_s/\hat{M}$ in the rotor frame.

2.2. *Periodicity*

We will now consider the periodicity of the unsteady wave fields which can exist in our cascade system. This issue has been discussed most famously by Tyler & Sofrin (1962), and only a brief description needs to be given here. Consider a single plane-wave component of the unsteady flow in the stator frame, say with velocity

potential

$$\phi \propto \exp(-\mathrm{i}K\tilde{x} - \mathrm{i}L\tilde{y} + \mathrm{i}nB\Omega_s^s t). \tag{2.2}$$

Here the $\tilde{x}, \tilde{y}$ axes are aligned with the face of the stator, as shown in figure 1. We note that the temporal periodicity of the flow forces the angular frequency of this wave to be an integer multiple, n, of the rotor blade passing frequency $B\Omega_s^s$. The wave field in the stator frame must be invariant when $\tilde{y}$ is increased by Δ and t is increased by Δ/Ω_s^s, corresponding to a given rotor blade rotating past one stator passage, and this leads immediately to Tyler & Sofrin's result

$$L = nB - mV \tag{2.3}$$

for integer m. The mode number m is essentially a spatial label of the plane-wave modes allowed in the gap for given n, and is exactly analogous to the index of the radiation modes in the non-rotating case described in (1). The temporal mode index n has arisen from the need to enforce temporal periodicity at the blade rotation rate, and has no counterpart in (1).

The inter-blade phase angle, corresponding to the change in phase of the unsteady field between adjacent leading edges in a given blade row, was seen to be an important quantity in (1), where it was denoted as σ. In the zero relative rotation case considered in (1), σ is the same for each blade row, but that is no longer the case when rotation is included. In the stator frame we denote the inter-blade phase angle as θ_n (to avoid notational confusion later), and it follows from (2.3), and from the fact that $\Delta = 2\pi/V$, that

$$\theta_n = -\frac{2n\pi B}{V}, \tag{2.4}$$

where an unimportant term $2\pi m$ has been removed. The suffix $_n$ makes it clear that the inter-blade phase angle depends on the temporal harmonic index.

In the frame rotating with the rotor each plane-wave component of the unsteady velocity potential is proportional to

$$\exp(-\mathrm{i}\hat{K}\hat{\tilde{x}} - \mathrm{i}\hat{L}\hat{\tilde{y}} + \mathrm{i}nV\Omega_s^r\hat{t}\,), \tag{2.5}$$

where the $\hat{\tilde{x}}, \hat{\tilde{y}}$ axes are aligned with the face of the rotor and are fixed in the rotating frame (see figure 1). By using the same approach as described above in the stator frame, we find that $\hat{L} = mB - nV$, and that the inter-blade phase angle in the rotor frame is

$$\hat{\theta}_n = \frac{2n\pi V}{B}. \tag{2.6}$$

The sign change between (2.4) and (2.6) has arisen from the fact that in the rotor frame the stator rotates in the negative $\hat{\tilde{y}}$-direction.

3. Wave field in the gap between blade rows

Just as in (1), the unsteady field in the gap between the blade rows consists of downstream- and upstream-propagating pressure waves and downstream-propagating vorticity waves. The amplitudes of all these modes are coupled together by the scattering at the blade leading and trailing edges, and we aim to determine the corresponding coupling matrices, which will then be analysed for resonance. Before doing this, however, we will write down general modal expressions for the field in the gap between the blade rows, as follows.

3.1. *Pressure waves*

Turning first to the pressure modes in the gap, the corresponding unsteady velocity potential, measured in the *stator* frame, can be written as a superposition of all possible fields of the form (2.2), i.e. summing over mode numbers m and n, in the form

$$\sum_n \sum_m \left(A_{nm} \mathrm{e}^{-\mathrm{i}\sigma^+_{nm} x - \mathrm{i}\lambda^+_{nm} y} + B_{nm} \mathrm{e}^{-\mathrm{i}\sigma^-_{nm} x - \mathrm{i}\mu^-_{nm} y} \right) \mathrm{e}^{\mathrm{i}nB\Omega^s_s t}, \tag{3.1}$$

where in keeping with (1) we have now chosen x, y axes aligned parallel and perpendicular to the stator-blade chords. The coefficients A_{nm} and B_{nm} are amplitudes of the upstream- and downstream-propagating acoustic modes in the gap, and the $\sigma^\pm_{nm}$, and λ^+_{nm} and μ^-_{nm} are the corresponding x- and y-wavenumbers respectively. By substituting the separate plane-wave components of (3.1) into the convected wave equation in the stator frame (i.e. with mean-flow Mach number M) and enforcing the condition that the stator transverse periodicity is given in terms of the inter-blade phase angle θ_n, we find that

$$\sigma^\pm_{nm} = \frac{d\,(2m\pi - \theta_n) - M^2 nB\Omega^s_s s^2 \mp \mathscr{S}}{d^2 + s^2\beta^2}, \tag{3.2}$$

where

$$\mathscr{S}^2 = s^2 \left(d^2 + s^2\right) M^2 n^2 B^2 \Omega^{s2}_s - 2dM^2 nB\Omega^s_s s^2 \,(2m\pi - \theta_n) - s^2\beta^2 (2m\pi - \theta_n)^2, \tag{3.3}$$

and $\mathscr{S} = |\mathscr{S}|$ when $\mathscr{S}^2 > 0$ and $\mathscr{S} = -\mathrm{i}|\mathscr{S}|$ when $\mathscr{S}^2 < 0$. Here $\beta^2 = 1 - M^2$. We note that this expression is very similar to the non-rotating result – equation (2.14) of (1) – the difference now being that the frequency and inter-blade phase angle depend on the temporal mode number n. In what follows we use the convention that n is always the first index on any of the variables or transmission matrices, indicating the harmonic of blade passing frequency at which the mode in question appears in the stator frame. By a simple coordinate transformation we can determine expressions for λ^+_{nm} and μ^-_{nm} in terms of $\sigma^\pm_{nm}$ respectively, with for instance

$$\mu^-_{nm} = \frac{nB - mV - \sigma^-_{nm} \cos\alpha}{\sin\alpha}, \tag{3.4}$$

and a similar result for λ^+_{nm}.

In the *rotor* frame the unsteady velocity potential of the pressure modes in the gap can be written in the form

$$\sum_n \sum_m \left(\hat{A}_{nm} \mathrm{e}^{-\mathrm{i}\hat{\sigma}^+_{nm}\hat{x} - \mathrm{i}\hat{\lambda}^+_{nm}\hat{y}} + \hat{B}_{nm} \mathrm{e}^{-\mathrm{i}\hat{\sigma}^-_{nm}\hat{x} - \mathrm{i}\hat{\mu}^-_{nm}\hat{y}} \right) \mathrm{e}^{\mathrm{i}nV\Omega^r_s \hat{t}}. \tag{3.5}$$

The various wavenumbers can be found by replacing the stator variables by the corresponding rotor variables in (3.2) and (3.4), so that for instance $M \to \hat{M}$, $\Omega^s_s \to \Omega^r_s$, $B \to V$; this final replacement arises from the fact that in the rotor frame the unsteady field can occur only at harmonics of the passing frequency of the V stator blades.

Of course, the fields described by (3.1) and (3.5) must be the same. This can easily be verified by making the transformation from stator to rotor frames

$$\hat{\tilde{y}} = \tilde{y} - \Omega^r_s \hat{t}, \tag{3.6}$$

and applying the periodicity arguments of § 2.2 we find that

$$\exp(-\mathrm{i}(nB - mV)\tilde{y} + \mathrm{i}nB\Omega^s_s t) \to \exp(-\mathrm{i}(nB - mV)\hat{\tilde{y}} + \mathrm{i}mV\Omega^r_s \hat{t}\,). \tag{3.7}$$

From this we can see that the mode indices are switched between the rotor and stator frames, so that the temporal mode n in the stator frame appears as the spatial mode n in the rotor frame, and vice versa. The amplitudes of the modes in (3.1) and (3.5) are then related by

$$e^{-i\hat{K}^{+}_{nm}g}\hat{A}_{nm} = \frac{M}{\hat{M}}A_{mn}, \quad e^{-i\hat{K}^{-}_{nm}g}\hat{B}_{nm} = \frac{M}{\hat{M}}B_{mn}, \tag{3.8}$$

where

$$\hat{K}^{+}_{nm} = \hat{\sigma}^{+}_{nm}\sin\hat{\alpha} - \hat{\lambda}^{+}_{nm}\cos\hat{\alpha}, \quad \hat{K}^{-}_{nm} = \hat{\sigma}^{-}_{nm}\sin\hat{\alpha} - \hat{\mu}^{-}_{nm}\cos\hat{\alpha}. \tag{3.9}$$

The term $\exp(-i\hat{K}^{\pm}_{nm}g)$ arises simply from the change in phase as the wave propagates (or decays) across the gap of width g, and the $\hat{K}^{\pm}_{nm}$ correspond to the resolved component of the phase in the direction perpendicular to the face of the cascade. The factor $M/\hat{M}$ arises from the fact that the unsteady velocity potentials have been normalized by different scales in the two frames.

3.2. *Vorticity waves*

The vorticity waves are shed from the trailing edge of each rotor blade so as to satisfy the unsteady Kutta condition there, and correspond to an upwash velocity in the direction normal to the blade chord, which convects with the local mean flow speed. Since we just need to know the upwash on the stators, it proves convenient to first determine the vortical upwash in the rotor frame on the plane of the rotor trailing edges, before transforming to the non-rotating frame and convecting the vorticity downstream. By comparison with (1.1) of (1), the upwash velocity in the y-direction for $(N-1)\hat{\Delta} < \hat{\bar{y}} < N\hat{\Delta}$, $N = 1, 2, \ldots, 2\pi/\hat{\Delta}$, can be written as a series of temporal harmonics in the form

$$\sum_n \hat{V}_n \cos(\hat{\alpha}-\alpha)\, e^{-inV\Omega^r_s(\hat{x}-N\hat{d})+inV\Omega^r_s\hat{t}+i\hat{\theta}_n N} f(\hat{y}-N\hat{s}). \tag{3.10}$$

We note that the phase of each vorticity wave simply corresponds to waves with temporal frequency $nV\Omega^r_s$ being convected with the local mean flow in the rotor frame – the appearance of the stator-blade number V here is of course due to the fact that it is the relative rotation of the stator which generates the unsteady field in the rotor frame. In (3.10) the vorticity wave amplitudes $\hat{V}_n$ are at this stage unknown, while the factor $\cos(\hat{\alpha}-\alpha)$ has arisen from resolving the upwash normal to the rotor blades into the y-direction. The function $f(\hat{y})$ describes the variation of the unsteady wakes perpendicular to the rotor blade chords, and can be obtained from the rotor trailing-edge scattering calculations described in § 3 of (1) and in Peake (1993); it turns out that

$$f(\hat{y}) = \frac{-i\hat{\gamma}\left(nV\Omega^r_s\right)e^{-i\hat{\gamma}\left(nV\Omega^r_s\right)\hat{y}}}{1-e^{-i\left(\hat{\theta}_n+nV\Omega^r_s\hat{d}+\hat{\gamma}\left(nV\Omega^r_s\right)\hat{s}\right)}} + \frac{i\hat{\gamma}\left(nV\Omega^r_s\right)e^{i\hat{\gamma}\left(nV\Omega^r_s\right)\hat{y}}}{1-e^{-i\left(\hat{\theta}_n+nV\Omega^r_s\hat{d}-\hat{\gamma}\left(nV\Omega^r_s\right)\hat{s}\right)}}. \tag{3.11}$$

Here $\hat{\gamma}\left(nV\Omega^r_s\right)$ can be found from the dispersion relation for the convected wave equation in the rotor frame, and corresponds to the (imaginary) $\hat{y}$-wavenumber of waves convecting with the (subsonic) mean flow speed – see equation (2.3) of (1).

The idea now is to resolve the temporal vorticity distribution along the rear face of the rotor into a series of spatial modes, so that (3.10) becomes, on $\hat{\bar{x}} = 0$,

$$\sum_n \sum_m \hat{\zeta}_{nm}\hat{V}_n \exp(i(nV-mB)\hat{\bar{y}}) \exp(inV\Omega^r_s\hat{t}\,), \tag{3.12}$$

and an expression for the Fourier coefficients $\hat{\zeta}_{nm}$ is derived in the Appendix. In order to find the upwash on the leading edge of the stators in the *stator* frame, we first transform (3.12) into the stator frame using (3.6). In the stator frame the vortical distribution convects in the x-direction with the stator mean-flow speed, and therefore in order to determine the upwash on stator blade zero we need to consider that part of the upwash from the rotor which is swept along the dash-dot line parallel to the stator blades in figure 1. This means that we need to evaluate the upwash distribution (3.12) on $\tilde{y} = -g/\tan\alpha$, and then introduce the extra phase term $\exp(-\mathrm{i}mB\Omega_s^s x)\exp(-\mathrm{i}mB\Omega_s^s g/\sin\alpha)$, where the first factor corresponds to the convected phase of the gust, and the second factor arises from the fact that the disturbance propagates over a distance $g/\sin\alpha$ from the rear face of the rotor to the leading edge of stator blade zero. All of this then yields the upwash on the zeroth stator blade in the form

$$\sum_n \sum_m V_{nm} \exp(\mathrm{i}nB\Omega_s^s t - \mathrm{i}nB\Omega_s^s x), \tag{3.13}$$

where

$$V_{nm} = \frac{\hat{M}}{M}\hat{\zeta}_{mn}\hat{V}_m \exp(-\mathrm{i}\hat{K}_{mn}^{\curlyvee} g). \tag{3.14}$$

Here

$$\hat{K}_{nm}^{\curlyvee} = \frac{nV - mB}{\tan\alpha} + \frac{mB\Omega_s^s}{\sin\alpha} \tag{3.15}$$

corresponds to the phase change experienced by the gust as it propagates to the stator, while the factor $\hat{M}/M$ in (3.14) has again risen from changing to the stator normalization. Note that in deriving (3.14) we have interchanged n and m, in order to retain n as the index of the time harmonic.

4. Stator and rotor scattering

We now analyse the interaction between the unsteady field in the gap and the rotor and stator, making very extensive use of the results derived in (1).

4.1. *Stator scattering*

In this subsection we consider the scattering of the downstream-propagating unsteady field in the gap between the two blade rows by the stator, in exact analogy to § 2 of (1). Essentially, we start by neglecting the stator trailing edges and considering just scattering by the leading edges. This involves determination of the field in the zeroth blade passage, $\phi_0(x, y, t)$, with the zero- normal-velocity boundary condition on $y = 0$

$$\frac{\partial \phi_0}{\partial y}(x, 0, t) - \sum_n \sum_m \left(\mathrm{i}\mu_{nm} B_{nm} \mathrm{e}^{-\mathrm{i}\bar{\sigma}_{nm} x} - V_{nm} \mathrm{e}^{-\mathrm{i}nB\Omega_s^s x}\right) \mathrm{e}^{\mathrm{i}nB\Omega_s^s t} = 0, \tag{4.1}$$

applied for all $x > 0$. The contribution to the upwash from the pressure waves comes from taking the y-derivative of the corresponding potential in (3.1), while the vortical gust component is taken straight from (3.13). We compare this equation with the corresponding boundary condition in (1); in that non-rotating case, only a single summation over the spatial modes was present, whereas now we have an additional temporal summation. In fact, taking the semi-infinite Fourier transform of (4.1) over $x > 0$ yields a condition which is exactly the same as equation (2.1) of (1), except for the introduction of this temporal summation. It therefore follows that the results

derived in (1) can be applied to the present case, with the unspecified frequency parameter Ω in (1) being set equal to $nB\Omega_s^s$ for each temporal harmonic. For instance, we find that the radiation reflected back upstream from the stator leading edges is written in the form

$$\sum_n \sum_m A_{nm} \mathrm{e}^{-\mathrm{i}\sigma_{nm}^+ x - \mathrm{i}\lambda_{nm}^+ y} \mathrm{e}^{\mathrm{i}nB\Omega_s^s t}, \tag{4.2}$$

where

$$A_{nm} = \sum_p \left(T_{npm}^{\mathscr{P}\mathscr{P}} B_{np} + T_{nm}^{\mathscr{V}\mathscr{P}} V_{np} \right), \tag{4.3}$$

and where the transmission matrices are given by

$$T_{npm}^{\mathscr{P}\mathscr{P}} = -\frac{\mathscr{K}^+(\sigma_{nm}^+)}{2(\sigma_{nm}^+ - nB\Omega_s^s)} \times Res^1_{\sigma_{nm}^+} \times \frac{\mu_{np}^- \mathscr{K}^-(\sigma_{np}^-)}{(\sigma_{nm}^+ - \sigma_{np}^-)}, \tag{4.4}$$

$$T_{nm}^{\mathscr{V}\mathscr{P}} = -\frac{\mathscr{K}^+(\sigma_{nm}^+)}{2(\sigma_{nm}^+ - nB\Omega_s^s)} \times Res^1_{\sigma_{nm}^+} \times \frac{\mathscr{K}^-(nB\Omega_s^s)}{(\sigma_{nm}^+ - nB\Omega_s^s)}, \tag{4.5}$$

and

$$Res^1_{\sigma_{nm}^+} = \frac{-\gamma\left(\sigma_{nm}^+\right)\left[\frac{1}{2}\left(\mathrm{e}^{\mathrm{i}\left(\theta_n + \sigma_{nm}^+ d\right)} - \mathrm{e}^{-\mathrm{i}\gamma\left(\sigma_{nm}^+\right)s}\right) + \frac{1}{2}\left(\mathrm{e}^{\mathrm{i}\left(\theta_n + \sigma_{nm}^+ d\right)} - \mathrm{e}^{\mathrm{i}\gamma\left(\sigma_{nm}^+\right)s}\right)\right]}{\gamma\left(\sigma_{nm}^+\right) d \sin\left(\theta_n + \sigma_{nm}^+ d\right) + s\left(M^2\Omega_n + \beta^2\sigma_{nm}^+\right) \sin\left(\gamma\left(\sigma_{nm}^+\right) s\right)}; \tag{4.6}$$

cf. (2.18), (2.19) and (2.16) of (1) respectively. The terms $\mathscr{K}^{\pm}$ correspond to Wiener–Hopf factors, which can be expressed in terms of infinite products, as described in Peake (1993). We again emphasize that all the above expressions are simply taken straight from (1), with only an entirely straightforward modification corresponding to summation over the temporal harmonics.

Having completed the leading-edge analysis, the inclusion of finite-chord effects can now be included, which essentially involves considering the additional upstream-propagating radiation produced by the scattering of the upstream-travelling stator duct modes by the stator leading edges. This is completed exactly as in (1), and the reader is referred there for full details. We find that the unknown amplitudes of the upstream-propagating pressure modes are still given by equation (4.3), but with the matrices $T_{npm}^{\mathscr{P}\mathscr{P}}$ and $T_{nm}^{\mathscr{V}\mathscr{P}}$ replaced by

$$T_{npm}^{\mathscr{P}} = T_{npm}^{\mathscr{P}\mathscr{P}} + T_{npm}^{\mathscr{P}\mathscr{D}\mathscr{P}}, \quad T_{nm}^{\mathscr{V}} = T_{nm}^{\mathscr{V}\mathscr{P}} + T_{nm}^{\mathscr{V}\mathscr{D}\mathscr{P}}. \tag{4.7}$$

Here the correction matrix $T_{npm}^{\mathscr{P}\mathscr{D}\mathscr{P}}$ describes the way in which the downstream-travelling pressure modes are scattered into downstream-travelling stator duct modes, which are then reflected and re-reflected arbitrarily many times in the stator passages between the leading and trailing edges, before being scattered into upstream-travelling pressure waves. The expression for $T_{npm}^{\mathscr{P}\mathscr{D}\mathscr{P}}$ can easily be constructed from the results in § 2 of (1), and we emphasize again that it represents an exact correction for finite-chord effects, which in particular contains the whole of the infinite reflection series in the stator blade passages. In the same way, the matrix $T_{nm}^{\mathscr{V}\mathscr{D}\mathscr{P}}$ describes the way in which the vorticity waves are scattered into downstream-travelling duct modes, which are then multiply reflected in the blade passages and rescattered into upstream-travelling pressure waves at the stator leading edges.

4.2. *Rotor scattering*

We now analyse the rotor trailing-edge scattering in the rotor-fixed frame of reference. We let $\hat{\phi}_0$ denote the scattered field due to the incidence of the $\hat{A}_{nm}$ on the trailing

edges of the upstream blade row; it follows that $\hat{\phi}_0$ is a solution of the convected wave equation in the rotor frame (Mach number $\hat{M}$). By ignoring the rotor leading edges in the first instance, the normal velocity boundary condition on rotor blade zero becomes

$$\frac{\partial \hat{\phi}_0}{\partial \hat{y}}(\hat{x},0) + \frac{\partial}{\partial \hat{y}} \sum_n \sum_m \hat{A}_{nm} \mathrm{e}^{-\mathrm{i}\hat{\sigma}^+_{nm}\hat{x} - \mathrm{i}\hat{\lambda}^+_{nm}\hat{y}} = 0 \tag{4.8}$$

for $\hat{x} < 0$. Again, this boundary condition is exactly analogous to the one used in § 3 of (1), except we now have the additional temporal summation over n. The other boundary condition is that the unsteady pressure must be continuous across the blade wake, together with the Kutta condition of zero pressure jump at the trailing edges. The problem can be solved using the Wiener–Hopf technique in exactly the same way as in (1). We therefore find that the temporal coefficients of the vorticity waves shed from the rotor trailing edges are

$$\hat{V}_n = \sum_m \hat{T}^{\mathscr{P}\mathscr{V}}_{nm} \hat{A}_{nm}, \tag{4.9}$$

while the amplitudes of the downstream-travelling pressure waves are

$$\hat{B}_{nm} = \sum_p \hat{T}^{\mathscr{P}\mathscr{P}}_{npm} \hat{A}_{np}. \tag{4.10}$$

Expressions for the matrices $\hat{T}^{\mathscr{P}\mathscr{V}}_{nm}$ and $\hat{T}^{\mathscr{P}\mathscr{P}}_{npm}$ can be inferred directly from equations (3.4) and (3.6), (3.7) of (1).

The next step is to include the finite rotor chord, and this is again completed in exactly the same way as in § 3.2 of (1). The final result is that the coefficients of the downstream-travelling vorticity and pressure in the rotor frame are given by equations (4.9) and (4.10) respectively, but with the matrices $\hat{T}^{\mathscr{P}\mathscr{V}}_{nm}$ and $\hat{T}^{\mathscr{P}\mathscr{P}}_{npm}$ replaced by $\hat{T}^{\mathscr{V}}_{nm}$ and $\hat{T}^{\mathscr{P}}_{npm}$, where

$$\hat{T}^{\mathscr{V}}_{nm} = \hat{T}^{\mathscr{P}\mathscr{V}}_{nm} + \hat{T}^{\mathscr{P}\mathscr{D}\mathscr{V}}_{nm}, \quad \hat{T}^{\mathscr{P}}_{npm} = \hat{T}^{\mathscr{P}\mathscr{P}}_{npm} + \hat{T}^{\mathscr{P}\mathscr{D}\mathscr{P}}_{npm}. \tag{4.11}$$

Here the matrix $\hat{T}^{\mathscr{P}\mathscr{D}\mathscr{P}}_{npm}$ describes the way in which the incident pressure modes are scattered into upstream-travelling duct modes in the rotor-blade passages, before being (multiply) reflected and re-reflected by the rotor leading and trailing edges, and finally being scattered by the trailing edges into downstream-travelling pressure waves in the gap. In the same way, $\hat{T}^{\mathscr{P}\mathscr{D}\mathscr{V}}_{nm}$ represents the conversion of incident pressure waves into vorticity waves via multiple reflections of duct modes in the rotor blade passages.

4.3. *Matrix equation*

Having analysed the way in which the field in the gap interacts with the rotor and stator blade rows, our aim is now to determine a single homogeneous matrix equation for one set of amplitudes (say the A_{nm}). To do this we start with equation (4.3) for A_{nm} in terms of the B_{nm} and V_{nm}, use (3.8) and (3.14) to rewrite the right-hand side in terms of the coefficients in the rotor frame, apply (4.10) and (4.9) to express $\hat{B}_{nm}$ and $\hat{V}_{nm}$ in terms of $\hat{A}_{nm}$, and then finally use (3.8) again to re-express the right-hand side back in terms of A_{nm}. This yields the matrix equation

$$A_{nm} = \sum_{p,q} \left\{ T^{\mathscr{P}}_{npm} \hat{T}^{\mathscr{P}}_{pqn} \exp(-\mathrm{i}g\hat{K}^-_{pn}) + T^{\mathscr{V}}_{nm} \hat{T}^{\mathscr{V}}_{pq} \hat{\zeta}_{pn} \exp(-\mathrm{i}g\hat{K}^{\mathscr{V}}_{pn}) \right\} \exp(\mathrm{i}g\hat{K}^+_{pq}) A_{qp}. \tag{4.12}$$

We can now analyse this equation for the occurrence of resonance, but in order to do this it will be necessary to truncate the infinite summations to finite order (just as in (1)), for both the spatial and temporal summations, and we will therefore suppose that all the summations run between $\mp N$ for fixed N (whose precise value will be chosen at a later stage). We can then write (4.12) in the general form

$$\sum_{k,l=-N}^{N} Q_{ijkl} A_{kl} = 0, \tag{4.13}$$

where

$$Q_{ijkl} = \left\{ T^{\mathscr{P}}_{jli} \hat{T}^{\mathscr{P}}_{lkj} \exp(-\mathrm{i}g\hat{K}^{-}_{pn}) + T^{\mathscr{S}}_{ji} \hat{T}^{\mathscr{S}}_{lk} \hat{\zeta}_{lj} \exp(-\mathrm{i}g\hat{K}^{\mathscr{S}}_{lj}) \right\} \exp(\mathrm{i}g\hat{K}^{+}_{lk}) - \delta_{il}\delta_{jk}. \tag{4.14}$$

The next step is to re-form the $(2N+1) \times (2N+1)$ amplitude matrix A_{kl} into the $(2N+1)^2$ length vector $\mathscr{A}_q$, $q = 1, 2, \ldots, (2N+1)^2$, which is completed by writing

$$\left.\begin{aligned} k &= -N + \mathrm{int}\left(\frac{q-1}{2N+1}\right), \\ l &= q - N - 1 - (2N+1)\mathrm{int}\left(\frac{q-1}{2N+1}\right). \end{aligned}\right\} \tag{4.15}$$

In this way the elements $A_{-N,l}$, $l = -N, \ldots, N$, form the first $l + N + 1$ elements of the vector $\mathscr{A}_q$, etc. Equivalently, the $(2N+1)^4$ elements Q_{ijkl} are formed into the $(2N+1)^2 \times (2N+1)^2$ matrix $\mathscr{Q}_{pq}$, using (4.15) together with

$$\left.\begin{aligned} i &= -N + \mathrm{int}\left(\frac{p-1}{2N+1}\right), \\ j &= p - N - 1 - (2N+1)\mathrm{int}\left(\frac{p-1}{2N+1}\right). \end{aligned}\right\} \tag{4.16}$$

This allows us to rearrange (4.12) into the form of the single matrix equation

$$\sum_{q} \mathscr{Q}_{pq} \mathscr{A}_q = 0; \tag{4.17}$$

the equations with $i = -N$, $j = -N, \ldots, N$ from (4.12) correspond to the first $2N+1$ equations in (4.17), etc. We can now proceed as in (1), and look for resonance of the system by seeking sets of parameter values for which the matrix $\mathscr{Q}_{pq}$ is close to singularity, as measured by the reciprocal condition number. Representative results are presented in the next section.

Finally, we note here that the modes with temporal harmonic zero in either the rotor or stator frame correspond to a steady perturbation to the flow in that frame. Such a perturbation cannot be handled using the techniques described in (1), and in any event will not generate an acoustic field in its own frame when scattered by the blade row. This steady perturbation really plays the same role as the potential field of each blade row in its own frame, which is certainly ignored in our analysis. We therefore proceed by ignoring all terms in the various matrices with zero time harmonic.

5. Results

The aim of this paper is to demonstrate how the formulation described in (1) can be extended to account for blade rotation, and a full parametric study for a wide range of operating conditions will not be completed here.

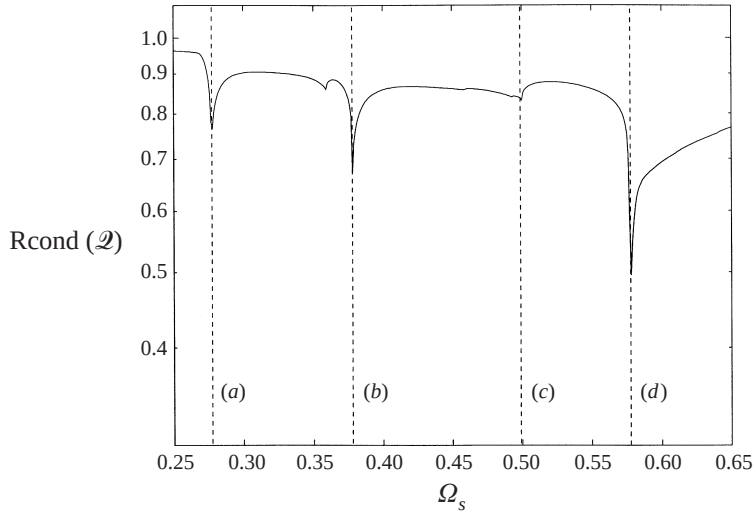

FIGURE 3. Reciprocal condition number, Rcond($\mathcal{Q}$), against shaft rotational frequency, Ω_s, showing the cut-on/cut-off mode frequencies at positions (*a*) Modes $n,m = [3,2],[3,4]$ and $[4,3]$, (*b*) Modes $n,m = [2,1],[2,3],[3,2],[3,4]$ and $[4,3]$, (*c*) Modes $n,m = [4,1]$ and (*d*) Modes $n,m = [1,2],[2,1],[2,3],[2,4]$ and $[4,2]$.

We first mention that the choice of matrix truncation number N is crucial. As N is increased the accuracy of the results for lower temporal harmonics will increase, but this is at the expense of introducing higher temporal harmonics with lower accuracy (although of course in practice the energy associated with each temporal harmonic decreases quite rapidly with increasing order). We believe that this limits the accuracy with which resonance can be determined, with the effect that it is very difficult to drive the reciprocal condition number to the sort of small values determined in (1). Moreover, as N is increased the number of elements in $\mathcal{Q}_{pq}$ increases like N^4. For these reasons it seems sensible to choose a moderate value of $N = 4$, which will typically include several cut-off modes at blade passing frequency. We also mention that the aim of our analysis is to predict the resonant frequencies themselves, rather than the behaviour of the system away from resonance. We find in our numerical calculations that the location of the excitations is insensitive to the precise value of N, although the behaviour away from these points may change a little with increasing N. However, for the reason stated above, such a variation is of little practical significance to us, and we believe that our choice of N here provides an accurate prediction of the excitation.

We first consider the relatively simple system studied by Kaji & Okazaki (1970), in which $B = V = 10$, $\alpha = \pi - \hat{\alpha} = \pi/3$ and $\Delta = \hat{\Delta} = g = \pi/5$. This leaves the shaft rate Ω_s to be varied, since once this has been specified the Mach numbers can be found from the velocity triangle in figure 2. In figure 3 the reciprocal condition number of $\mathcal{Q}_{pq}$ is plotted against Ω_s, here with the finite-chord effects neglected (simply achieved by neglecting the correction matrices $T^{\mathcal{PQP}}$ etc.). The system displays some evidence of weak excitation at the points (*a–d*), which all correspond to points at which one or more of the radiation modes in the gap between the blade rows are exactly cut off. These cut off frequencies can be found, for the stator, by setting $\sigma^+_{nm} = \sigma^-_{nm}$, and similarly for the rotor; in general, the cut-off frequencies for the two rows are different, but match in the highly symmetric case considered in the figure. The excitation level

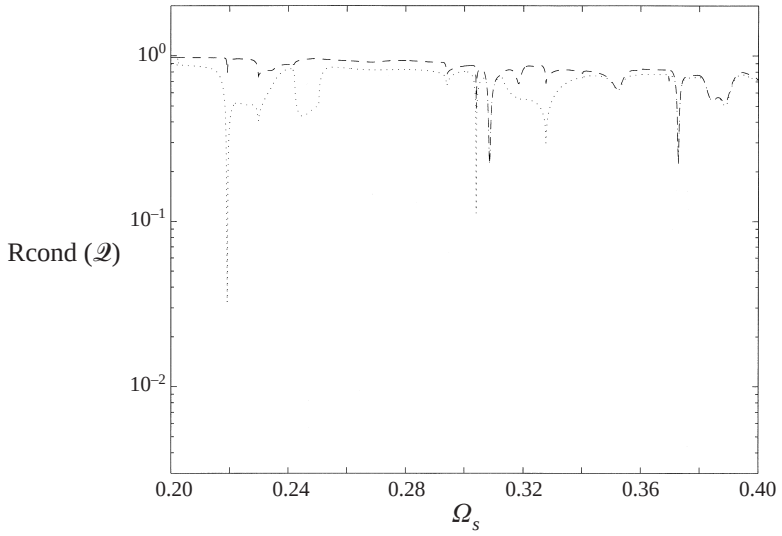

FIGURE 4. Reciprocal condition number, Rcond($\mathcal{Q}$), against shaft rotational frequency, Ω_s, for infinite–finite(dashed) and finite–finite(dotted) rotor–stator blades.

is seen to be higher at the points where more modes are cut off. We note, however, that the very clear-cut resonances observed in (1) are no longer present in the rotating case, which is perhaps in part due to the the errors involved in increasing the number of temporal harmonics.

In figure 4 we consider the system with $\alpha = \pi/4$, $\hat{\alpha} = 9\pi/20$, and with the pitch-to-chord ratio for the rotor and stator equal to 1 and 1/2 respectively, and plot the reciprocal condition number against Ω_s for two possible combinations of infinite/finite rotor/stator chords. The excitation at $\Omega_s \approx 0.37$ occurs at a frequency 1×BPF (i.e. it is the $n = 1$ temporal mode which is excited), and corresponds to a Parker resonance of the stator, which must be driven by the vorticity waves from the rotor. In fact, since $B = V$ it follows from (2.4) that the stator inter-blade phase angle is an integer multiple of 2π, so that this is a genuine Parker resonance as described in Parker (1966, 1967). In (1) the excitations observed occurred at real frequencies, and this is again true here, since our temporal modal representation forces the field to be composed of integer multiples of the corresponding blade passing frequency. The excitation therefore corresponds to a genuine, undamped trapped mode. The other two excitations in figure 4 ($\Omega_s \approx 0.22$, which occurs at 3×BPF, and $\Omega_s \approx 0.3$, which occurs at 2×BPF) are caused by an effect which we have not previously mentioned, whereby two duct modes, in either the rotor or stator blade passages, coalesce. Following the notation used in (1), the duct modes at time harmonic n are denoted $k^{\pm}_{nm}$, where the $\pm$ modes propagate upstream and downstream respectively, and this coalescence condition is $k^{+}_{nm} = k^{-}_{nm}$ for some n, m, or equivalently these duct modes are exactly cut off (both cases mentioned above correspond to $m = 1$). We note that our analysis breaks down here (since our formulation assumes that the leading and trailing edges of the rotor or stator blades communicate via duct modes propagating between them), but the enhanced excitation observed in figure 4 near these points indicates that this condition might well have some practical significance. We can also see in figure 4 that there is little excitation of the system at low Ω_s except when both blade rows have finite chords; the corresponding curves for infinite–infinite and

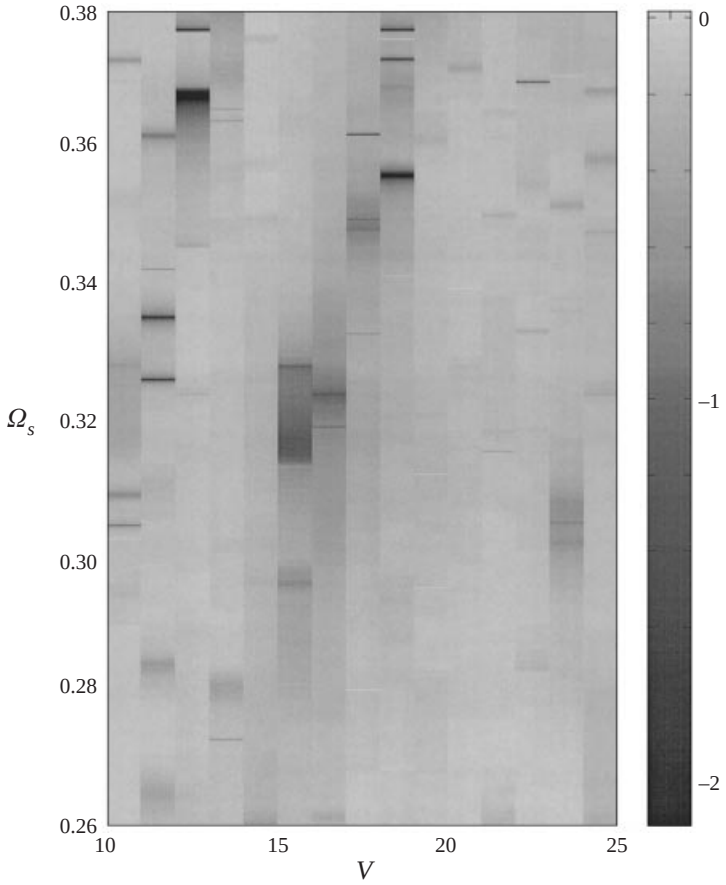

FIGURE 5. Logarithm of reciprocal condition number, $\log_{10}\mathrm{Rcond}(\mathcal{Q})$, as a function of stator vane number, V, and shaft rotational frequency, Ω_s.

finite–infinite chords are not plotted, but also show very little excitation indeed at low Ω_s. This behaviour is entirely to be expected: at low Ω_s, the radiation modes in the gap at a given temporal frequency tend to be cut off, and the excitation of the stator can only be driven by the vorticity shed from interaction between downstream-propagating duct modes and the rotor trailing edges, which in turn can only be included when the genuinely finite rotor chord is included.

In figure 5 we keep $B = 10$, but vary the stator vane number V (in practice the vane number is very often chosen to be larger than the blade number). Here we have genuine finite chords on both blade rows, and the results from figure 4 are repeated on the left-hand edge of figure 5. The duct mode cut-off excitation observed at just above $\Omega_s = 0.3$ in figure 4 is also seen to persist (weakly) for V larger than 10 (particularly for $V = 16, 23$). The Parker-mode excitation of the stator can be seen at $V = 10, \Omega_s \approx 0.37$. Another type of excitation can occur when two duct modes in the rotor coalesce, i.e. $\hat{k}^+_{nm} = \hat{k}^-_{nm}$. With $V = 15$ and for the temporal and spatial harmonics (in the rotor frame) $m = n = 2$, we find that this occurs for $\Omega_s \approx 0.313$, and this region of excitation can clearly be seen in figure 5. As well as the excitation points mentioned here, a number of other areas in which the reciprocal condition number becomes small can be observed in figure 5, but it has not proved possible to identify

other physical mechanisms which might be responsible. We note, however, that the partial excitations observed with semi-infinite blades when some radiation mode is exactly cut off cannot be identified for the genuine finite-chord system, equivalent to the behaviour of the non-rotating system described in (1).

6. Concluding remarks

In this paper we have shown how our analysis of the twin cascade in (1) can be extended to account for non-zero relative rotation. Possible excitation has again been identified, and mechanisms which have been identified include the Parker-like resonance of the stator, driven by the downstream-travelling acoustic or vorticity waves, and coincidence of duct modes in either the rotor or stator. Presumably, a Parker-like resonance of the rotor, driven by upstream-propagating acoustic waves from the stator, can also potentially occur.

Predictions of the natural resonant frequencies of the rotor–stator system can be combined with estimates of the vortex-shedding frequency to predict 'ladder diagrams' for the occurrence of acoustic resonance. Typically, as some flow parameter is increased (such as the axial speed), the shedding will lock onto successively higher natural modes, with the coincidences between the shedding frequency and natural frequencies delineating the parameter range over which a given mode is excited. An example of a sample prediction for the data from Legerton (1992) described in (1) is given in Woodley & Peake (1998), in which the present theory is combined with approximate predictions of the shedding frequency for a cascade (Woodley & Peake 1997). In order to determine which mode is excited, it turns out that the shedding frequencies need to be predicted exceedingly accurately, particularly at higher flow speeds, given the increasing modal density of the system. Indeed, we believe that while the predictions of natural frequency described here and in (1) are acceptable, the accuracy of predictions of vortex shedding frequencies needs to be considerably improved before completely reliable predictions of the onset of resonance can be made.

In addition to the resonance studied here, our analytical formulae can be used to study the acoustic response of a rotor–stator system to external forcing, possibly by wakes shed from some upstream engine stage. In that case, inhomogeneous equations for the various modal amplitudes can be derived, but the left-hand sides of these equations will necessarily be entirely equivalent to what has been presented in this paper.

The authors are grateful for financial support provided by EPSRC and Rolls-Royce plc, and to Dr A. B. Parry for helpful conversations.

Appendix

In this Appendix we re-express the vorticity waves shed from the rotor as a series of spatial and temporal harmonics. Along the rear face of the rotor $\hat{\hat{x}} = 0$ we have that the upwash in $(N-1)\hat{\Delta} < \hat{\hat{y}} < N\hat{\Delta}$ is, from (3.10),

$$\sum_n \hat{V}_n F_n(\hat{\hat{y}}) \mathrm{e}^{\mathrm{i}nV\Omega_s^r \hat{t}}, \tag{A 1}$$

where

$$F_n(\hat{\hat{y}}) = \cos(\hat{\alpha} - \alpha)\, \mathrm{e}^{-\mathrm{i}nV\Omega_s^r\left(\hat{\hat{y}}\cos\hat{\alpha} - N\hat{d}\right) + \mathrm{i}\hat{\theta}_n N} f\left(\hat{\hat{y}}\sin\hat{\alpha} - N\hat{s}\right). \tag{A 2}$$

In order to write down an expression which is valid for all $\hat{\bar{y}}$, we first note that to satisfy periodicity round the rotor annulus such an expression must take the form (see the expression for $\hat{L}$ following equation (2.5))

$$\sum_n \sum_m \hat{V}_n \hat{\zeta}_{nm} \exp\left(-\mathrm{i}(mB - nV)\hat{\bar{y}}\right) \exp(\mathrm{i}nV\Omega_s^r \hat{t}\,). \tag{A 3}$$

Considering each time harmonic separately, we now multiply this equation by $\exp(\mathrm{i}(pB - nV)\hat{\bar{y}})$ and integrate over $0 < \hat{\bar{y}} < 2\pi$, and then splitting the integration range up into B intervals of length $\hat{\Delta}$ and applying a simple coordinate transformation to each integral we find that

$$\hat{\zeta}_{np} = \frac{1}{2\pi} \sum_{r=0}^{B-1} \mathrm{e}^{\mathrm{i}r\hat{\theta}_n + \mathrm{i}(pB-nV)r\hat{\Delta}} \int_0^{\hat{\Delta}} F_n(\xi) \mathrm{e}^{\mathrm{i}(pB-nV)\xi} \mathrm{d}\xi. \tag{A 4}$$

We now substitute for $F_n(\xi)$ from (3.10), and then for the wake width function f from (3.11). Two standard integrals can then be completed, and after some algebra we find that

$$\hat{\zeta}_{np} = \frac{1}{2\pi} \sum_{r=0}^{B-1} \mathrm{e}^{\mathrm{i}r\left(\hat{\theta}_n + (pB-nV)\hat{\Delta}\right)} \cos(\hat{\alpha} - \alpha) \left[I_{np,1} + I_{np,2}\right], \tag{A 5}$$

where

$$I_{np,1} = \frac{\mathrm{e}^{\mathrm{i}\left((pB-nV) - nV\Omega_s^r \cos\hat{\alpha} - \hat{\gamma}\left(nV\Omega_s^r\right)\sin\hat{\alpha}\right)\hat{\Delta}} - 1}{\mathrm{i}\left((pB-nV) - nV\Omega_s^r \cos\hat{\alpha} - \hat{\gamma}\left(nV\Omega_r^s\right)\sin\hat{\alpha}\right)} \times \frac{-\mathrm{i}\hat{\gamma}\left(nV\Omega_s^r\right)}{1 - \mathrm{e}^{-\mathrm{i}\left(\hat{\theta}_n + nV\Omega_s^r\hat{d} + \hat{\gamma}\left(nV\Omega_s^r\right)\hat{s}\right)}},$$

$$I_{np,2} = \frac{\mathrm{e}^{\mathrm{i}\left((pB-nV) - nV\Omega_s^r \cos\hat{\alpha} + \hat{\gamma}\left(nV\Omega_s^r\right)\sin\hat{\alpha}\right)\hat{\Delta}} - 1}{\mathrm{i}\left((pB-nV) - nV\Omega_s^r \cos\hat{\alpha} + \hat{\gamma}\left(nV\Omega_s^r\right)\sin\hat{\alpha}\right)} \times \frac{\mathrm{i}\hat{\gamma}\left(nV\Omega_s^r\right)}{1 - \mathrm{e}^{-\mathrm{i}\left(\hat{\theta}_n + nV\Omega_s^r\hat{d} - \hat{\gamma}\left(nV\Omega_s^r\right)\hat{s}\right)}}.$$

REFERENCES

Hanson, D. B. 1992 Unsteady coupled cascade theory applied to the rotor/stator interaction noise problem. *AIAA Paper* 92-02-084.

Hanson, D. B. 1993 Mode trapping in coupled 2D cascades — acoustic and aerodynamic results *AIAA Paper* 93-4417.

Hanson, D. B. 1997 Acoustic reflection and transmission of rotors and stators including mode and frequency scattering. *AIAA Paper* 97-1610.

Kaji, S. & Okazaki, T. 1970 Propagation of sound waves through a blade row. *J. Sound Vib.* **11**, 355–375.

Legerton, M. L. Flow induced acoustic resonances. PhD Thesis, University of Swansea, UK.

Linton, C. M. & McIver, P. 1998 Acoustic resonances in the presence of radial fins in circular cylindrical waveguides. *Wave Motion* **28**, 99–117.

Parker, R. 1966 Resonance effects in wake shedding from parallel plates: some experimental observations. *J. Sound Vib.* **4**, 62–72.

Parker, R. 1967 Resonance effects in wake shedding from parallel plates: some experimental observations: calculation of resonant frequencies. *J. Sound Vib.* **5**, 330–343.

Peake, N. 1992 The interaction between a high-frequency gust and a blade row. *J. Fluid Mech.* **241**, 261–289.

Peake, N. 1993 The scattering of vorticity waves by an infinite cascade of flat plates in subsonic flow. *Wave Motion* **18**, 255–271.

Tyler, J. M. & Sofrin, T. G. 1962 Axial flow compressor noise studies. *SAE Trans.* **70**, 309–332.

Woodley, B. M. & Peake, N. 1997 Vortex shedding from a cascade of aerofoils. *AIAA Paper* 97-1814.

Woodley, B. M. & Peake, N. 1998 Prediction of acoustic resonance in tandem cascades. *AIAA/CEAS Paper* 98-2252.

Woodley, B. M. & Peake, N. 1999 Resonant acoustic frequencies of a tandem cascade. Part 1. Zero relative motion. *J. Fluid Mech.* **393**, 215–240.